Performance Evaluation of High-Voltage Underground Cables: Comparative Study of Copper and Aluminum Conductors

Jesus E. Guevara Asorza
University of Campinas
Campinas, Brazil
j272296@dac.unicamp.br

Ricardo A. de Araujo
Federal University of Lavras
São Sebastião do Paraíso, Brazil
ricardo.araujo@ufla.br

Theofilos A. Papadopoulos
Aristotle University of Thessaloniki
Thessaloniki, Greece
thpapad@ece.auth.gr

José Pissolato Filho
University of Campinas
Campinas, Brazil
pisso@unicamp.br

***Abstract*—In the selection of high-voltage underground cables, two fundamental electrical requirements must be satisfied: cable ampacity and induced sheath voltage levels. In practice, this verification is commonly performed using catalog data. When these requirements are not met, ampacity may be improved through the application of thermal backfill, whereas induced sheath voltages are largely determined by the adopted bonding method. However, systematic studies on the influence of cable type and conductor material on these parameters remain limited. This paper addresses this gap by analyzing copper- and aluminum-conductor cables under various installation scenarios. Results show that, for equal cross-sectional areas, copper conductors provide on average 185 A higher ampacity than aluminum, but also result in higher induced sheath voltages, potentially affecting personal safety. Moreover, thermal backfill and wider cable spacing can reduce the required cross-sectional area of HV cables.**

***Index Terms*—Ampacity, high-voltage cable, induced cable sheath voltages, sheath bonding methods.**

I. Introduction

Selecting high-voltage (HV) underground cables is a complex task, as multiple requirements and design options must be considered. Thermal performance, electrical characteristics, mechanical reliability, installation constraints, and economic factors interact in intricate ways [1], rendering the cable design and specification process a multidimensional engineering problem. Among these considerations, two electrical parameters are particularly critical: determining the cable ampacity and calculating the induced voltages on the metallic sheaths.

Ampacity calculations for HV cables are traditionally based on the IEC 60287 Std. [2], which relies on a number of simplifications and assumptions that may not always yield accurate results. To address these limitations, CIGRE TB 880 [3] provides guidelines for benchmarking ampacity cases. However, these approaches limit the consideration of low-thermal-resistivity backfill [4], a material that enhances cable ampacity, to a single layer surrounding the cables. In practice, additional constraints often apply, such as the need for high mechanical protection provided by a concrete duct bank with an additional controlled backfill layer above it. This configuration is common in urban installations [5], [6]. In such cases, where the IEC 60287 Std. may not be directly applicable, sophisticated simulation tools such as CYMCAP [7], ELEK High-Voltage Cable [8], and COMSOL [9] can be employed to perform accurate ampacity assessments [5], [10], [11].

Induced voltages on cable sheaths arise from both inductive and capacitive coupling between the cable conductor, the sheath, and adjacent cables. Inductive coupling is the dominant mechanism, while capacitive effects become increasingly significant over long distances [12]. Since inductive coupling is governed by Faraday's law, higher conductor currents result in higher induced sheath voltages. Analytical expressions for induced voltages are provided by IEEE 575 [13] and CIGRE 283 [14], but these formulations neglect the contribution of self-earth return impedance [15], which can lead to discrepancies when compared with electromagnetic transient (EMT) simulations [12], [16].

While methodologies for evaluating cable ampacity and induced sheath voltages are well established, most studies assume fixed HV cable types. A systematic assessment of the influence of cable type, particularly conductor material (copper or aluminum) and cross-sectional area, on ampacity and induced sheath voltages remains unexplored.

The novelty of this study is the comprehensive assessment of HV cable performance, in terms of ampacity and sheath-induced voltages, for multiple cable types and cross-sections installed in duct banks. By systematically evaluating the influence of backfill thermal properties, natural soil thermal resistivity, and cable spacing, the work reveals conditions under which cables with markedly different designs can deliver comparable operational performance. These results contribute to a deeper understanding of cable system optimization in practical engineering applications.

II. Ampacity for underground HV cables

Cable ampacity refers to the maximum current that a cable can carry, either when buried directly in the ground or installed in ducts, without exceeding the maximum operating

This work was supported by São Paulo Research Foundation (FAPESP) (grants: 2021/11258-5 and 2023/05066-1).

979-8-3315-8138-1

temperature specified by the manufacturer [17]. For cables insulated with cross-linked polyethylene (XLPE), this limit is typically 90 °C [18]. The ampacity calculation is based on a thermal balance considering the cable internal components and the external environment characteristics. When the thermal resistivity of the surrounding media is high, heat dissipation from the trench becomes more difficult, resulting in increased cable temperatures. Moreover, if additional heat sources are present in the external medium, such as a neighboring circuit, these must be accounted for in the analysis, as they further contribute to the overall thermal loading of the installation.

In recent years, one of the most common methods to increase cable ampacity has been the use of thermal backfill, which is a material with low thermal resistivity compared to the natural ground [19], which is installed above the duct bank or above the cables. Evaluating the impact of backfill on the cable ampacity requires solving heat transfer equations, typically through the finite element method (FEM). Commercial software such as CYMCAP [7] implements this type of analysis. The cable ampacity, according to [2], is given by (1),

$$I = \left[\frac{\Delta\theta - W_d \left(0.5 T_1 + n \left(T_3 + T_4\right)\right)}{R_c T_1 + n R_c \left(1 + \lambda_1\right) \left(T_3 + T_4\right)} \right]^{0.5} \tag{1}$$

which determines the current that produces a temperature rise, $\Delta\theta$, within the cable. The temperature increase depends on the conductor AC resistance at the operating temperature and on the thermal resistances of the surrounding materials, such as ducts, backfill, concrete, and other layers. For single-core cables without armor, these thermal resistances in (1) are denoted as T_1, T_3, and T_4, corresponding to the insulation, the outer covering, and the external medium, respectively, and are expressed in $K\mathrm{mW}^{-1}$. In the case of cables installed inside duct banks, T_4 is subdivided into three components: $T_4^{'}$, $T_4^{''}$, and $T_4^{'''}$, representing the thermal resistance of the medium inside the duct (pipe), the pipe wall itself, and the surrounding environment, respectively. The latter component is typically determined through FEM-based calculations. Furthermore, the ratio of sheath losses to total conductor losses, λ_1, is defined as the sum of losses due to circulating currents in the sheath, $\lambda_1^{'}$, and those arising from eddy currents, $\lambda_1^{''}$.

III. Calculation of Induced Sheath Voltages

For this study, the calculation of induced voltages on the cable sheath is derived from the series impedance formulation presented in (2), based on [15], [20], which assumes inductive current on cable sheath equal to zero.

$$\begin{bmatrix} V_{SA} \\ V_{SB} \\ V_{SC} \end{bmatrix} = \begin{bmatrix} Z_{cs,1} + Z_{gs,1} & Z_{gm,12} & Z_{gm,13} \\ Z_{gm,12} & Z_{cs,2} + Z_{gs,2} & Z_{gm,23} \\ Z_{gm,13} & Z_{gm,23} & Z_{cs,3} + Z_{gs,3} \end{bmatrix} \begin{bmatrix} I_A \\ I_B \\ I_C \end{bmatrix} \tag{2}$$

where $Z_{gm,ij}$ represents the mutual impedance between cable i and j, $Z_{cs,i}$ is the impedance between core and sheath of cable i and $Z_{gs,i}$ is the self-earth return impedance of cable i.

When cables are installed inside ducts, assumed as high-density polyethylene (HDPE) in this study, the effect of the HDPE pipes can be modeled through a modified effective permittivity of the sheath insulation, as described in [21]. This adjustment directly affects the capacitive coupling between cables; however, its influence on the induced voltage calculation at power frequency is almost negligible. Therefore, only inductive coupling is considered in this study.

IV. Results

HV copper and aluminum-conductor cables with different cross-sections were systematically analyzed to assess their steady-state performance, specifically regarding ampacity and induced sheath voltages. The main electrical and geometrical parameters, summarized in Table I [22], correspond to a 220 kV underground transmission line. Each single-core cable, as shown in Fig. 1, includes a metallic sheath of copper wires with an aluminum laminated foil (150 mm^2), semi-conductive layers for electric field control, 21 mm XLPE insulation, and a polyethylene jacket. As shown in Table I, copper-conductor cables present higher weight and greater pulling force than aluminum-conductor alternatives. Moreover, an ideal cross-bonding sheath configuration was assumed for all cables, meaning that circulating currents in cable sheaths were neglected.

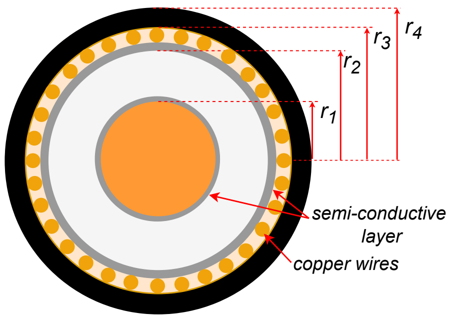

Fig. 1. Single-core cable at 220 kV

The analyzed HV single-core cables are arranged in a flat configuration and installed within HDPE pipes, whose internal and external radii are 220 and 250 mm, respectively. The ducts are embedded in a concrete with a thermal resistivity, ρ_c, equal to 0.75 KmW^{-1} [20]. Above the concrete structure, a controlled backfill layer with a thermal resistivity, ρ_b, equal to 0.9 KmW^{-1} [20] is used, as illustrated in Fig. 2 for increasing the HV cable ampacity. The surrounding natural soil is modeled by its thermal resistivity, denoted as ρ_n. $h_{backfill}$ is the depth of the duct where the backfill is employed. h_{ins} is the depth of installation of the duct bank. The detailed geometrical characteristics of the duct bank are summarized in Table II, based on [1]. A daily load factor (DLF) of 0.85 and an ambient temperature of 34 °C were assumed for all simulations.

A. Ampacity results

For the ampacity calculation of the HV cables, the CYMCAP software was employed, owing to its recognized accuracy and capability to explicitly account for the thermal contribution of the backfill in the simulations.

To analyze the impact of ρ_n on the ampacity performance for both cable conductor materials, $h_{backfill}$ and h_{ins} were set to 1.2 m. Different conductor cross-sectional areas, ranging

979-8-3315-8138-1

TABLE I
INPUT DATA OF SINGLE-CORE CABLES

Material	Section (mm^2)	Diameter of conductor (mm)	Diameter over insulation (mm)	Diameter over sheath (mm)	Outer diameter of cable (mm)	Resistance of conductor at 90°C (Ω/km)	Cable weight (kg/km)	Maximum pulling force (kN)
Copper	1000	38.3	82.9	89.5	100	0.0275	16400	50
	1200	41.6	87.8	94.4	105	0.0222	18760	60
	1400	45.8	92	98.6	109	0.0198	20790	70
	1600	49.6	95.8	102.4	113	0.0182	23120	80
	1800	53.2	99.4	106	117	0.0169	25650	90
	2000	54.6	100.8	107.4	119	0.0158	27220	100
Aluminum	1000	38	82.6	89.2	99	0.0408	10050	35
	1200	43	89.2	95.8	106	0.0319	11380	42
	1400	45.1	91.3	97.9	109	0.0275	12140	49
	1600	48.5	94.7	101.3	112	0.0242	13050	56
	1800	52.7	98.9	105.5	117	0.0216	14110	63
	2000	54.5	100.7	107.3	119	0.0195	14780	70

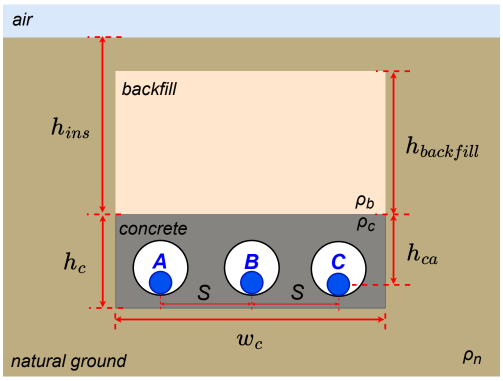

Fig. 2. Duct bank configuration

TABLE II
DUCT BANK DIMENSIONS

Configuration	S (mm)	H_c (mm)	W_c (mm)
Flat	300	435	950
	350	435	1050
	400	435	1150
	450	435	1250

from 1200 to 1800 mm^2, were evaluated, as illustrated in Fig. 3, considering S equal to 300 mm.

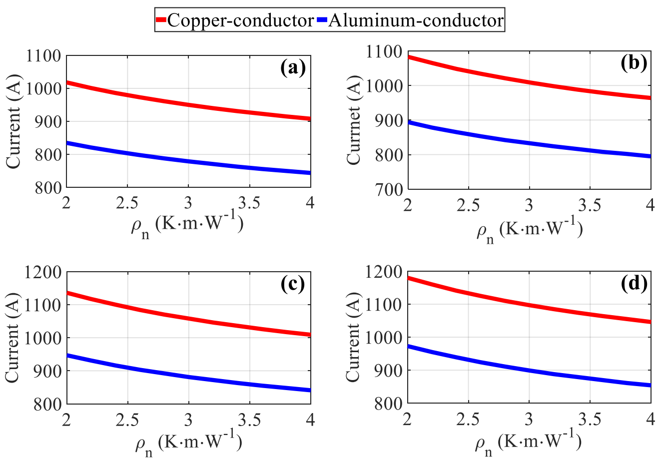

Fig. 3. Ampacity in function of ρ_n. (a) 1200 mm^2, (b) 1400 mm^2, (c) 1600 mm^2, and (d) 1800 mm^2.

Fig. 3 clearly illustrates that ampacity increases with the conductor cross-sectional area, while it decreases as the soil thermal resistivity, ρ_n, becomes higher. Copper-conductor cables consistently exhibit superior ampacity to those with aluminum conductors. Remarkably, a copper-conductor cable with a cross-section of 1200 mm^2 achieves higher ampacity than an aluminum-conductor cable with a cross-section of 1800 mm^2, highlighting the significant influence of the conductor material on current-carrying capability.

Unlike overhead conductors, where an increase in current demand is typically addressed by enlarging the conductor cross-section, underground cables offer an additional design degree of freedom: the spacing between adjacent cables. Increasing this separation reduces the effective external thermal resistivity, enhancing heat dissipation and improving current-carrying capacity [5]. Therefore, Fig. 4 illustrates the ampacity behavior for different cable cross-sections, varying S, considering a natural soil thermal resistivity of ρ_n = 2.6 KmW^{-1} and a $h_{backfill}$ equal to 1.2 m.

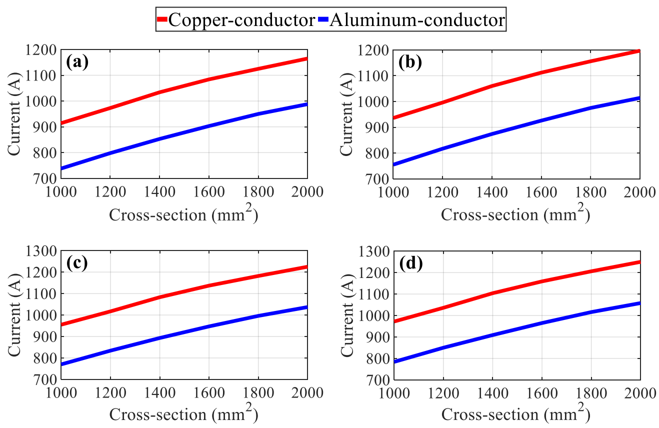

Fig. 4. Ampacity in function of cross-section cable, varying S. (a) 300 mm, (b) 350 mm, (c) 400 mm, and (d) 450 mm.

Fig. 4 reveals that copper-conductor cables exhibit higher ampacity than those with an aluminum conductor with the same cross-section area, on average, approximately 185 A. As cable spacing increases, the required cross-sectional area can be reduced. For instance, for a nominal current of 900 A, several options are possible: an aluminum-conductor cable with a 1600 mm^2 cross-section at S = 300 mm, an aluminum-conductor cable with a 1400 mm^2 cross-section at S = 450 mm, or a copper-conductor cable with a 1000 mm^2 cross-section at S = 300 mm. These results emphasize the significant influence of separation between cables on

979-8-3315-8138-1

ampacity calculations, which can directly affect conductor sizing. However, increasing S also entails higher costs and longer construction times for duct banks. Therefore, a techno-economic analysis is required to determine whether enlarging the duct bank dimensions is justified.

The backfill material also plays a significant role in ampacity analysis. In many cases, it is not necessary to place a large depth of backfill above the duct banks; even a partial layer may be sufficient. Figs. 5 and 6 show the effect of $h_{backfill}$ on the ampacity, measured from the top of the duct bank to the ground surface, for cables with copper and aluminum conductors, respectively. In these results, the ρ_n is assumed as 2.6 KmW^{-1}. For $h_{backfill}$ values lower than the duct bank installation depth, the remaining space is filled with the natural ground.

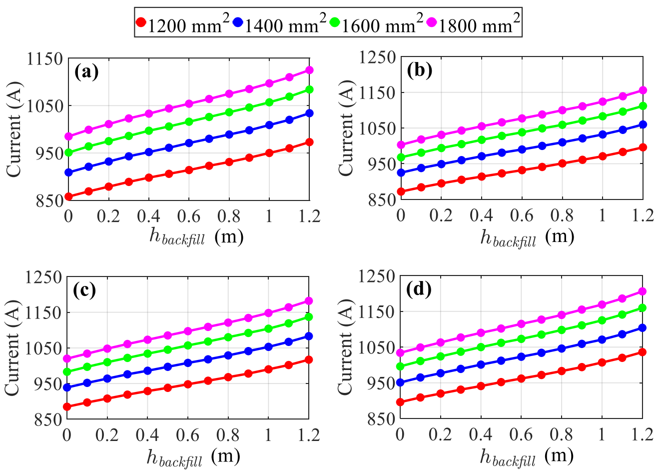

Fig. 5. Ampacity in function of $h_{backfill}$ for cable with copper-conductor varying S. (a) 300 mm, (b) 350 mm, (c) 400 mm, and (d) 450 mm.

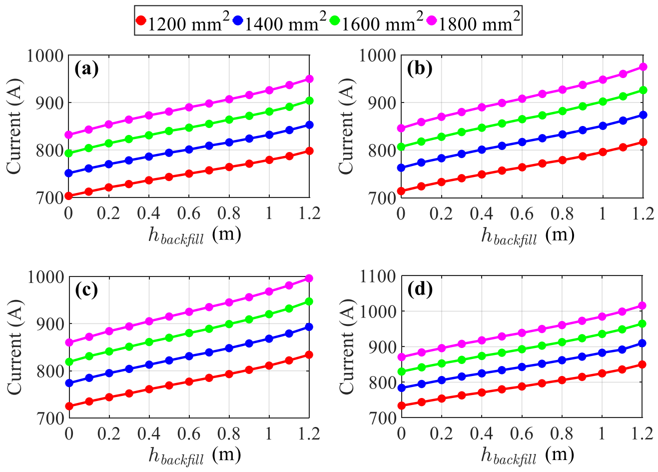

Fig. 6. Ampacity in function of $h_{backfill}$ for cable with aluminum-conductor varying S. (a) 300 mm, (b) 350 mm, (c) 400 mm, and (d) 450 mm.

A higher $h_{backfill}$ improves heat dissipation toward the surface, allowing higher current to flow in the cable conductor without exceeding the temperature limit. This effect becomes more significant for larger cross-sections. For instance, a copper-conductor cable with a cross-section of 1200 mm^2 and S = 300 mm has an ampacity of 858 A without backfill. When $h_{backfill}$ is 1.2 m, the ampacity increases to 973 A, which is a gain of 115 A (13.4%). For the same S and a cross-section of 1800 mm^2, the ampacity increases from 985 A (no backfill) to 1125 A (with $h_{backfill}$ = 1.2 m), an increment of 140 A (14.2%), which for this voltage level corresponds to 9 MW extra, approximately. Additionally, increasing S further improves ampacity performance, since a larger volume of backfill is installed. Considering the same 1200 mm^2 copper-conductor cable but with S = 450 mm, the ampacity goes from 896 A (without backfill) to 1036 A (with $h_{backfill}$ = 1.2 m), yielding a gain of 140 A, equivalent to a 15.6% increase compared to the case with S = 300 mm. A similar trend is observed when comparing the gain generated by the backfill between copper- and aluminum-conductor cables. For instance, an aluminum-conductor cable with a cross-section of 1200 mm^2 and S equal to 300 mm increases its ampacity from 703 A (without backfill) to 798 A (with $h_{backfill}$ = 1.2 m), a gain of 98 A, which is lower than the improvement obtained with a copper-conductor cable under the same conditions. Overall, copper-conductor cables exhibit superior ampacity performance compared to aluminum-conductor cables when backfill is employed.

Considering a nominal current requirement of 950 A, several alternatives can be identified. These include variations in conductor material, cross-sectional area, and S, as well as the possibility of reducing $h_{backfill}$. For the specified current, one option with a copper-conductor conductor is a cable with a 1200 mm^2 cross-section, installed with $S = 300$ mm and a backfill thickness $h_{backfill} \geq 1.0$ m. An alternative configuration involves the same cable with $S = 0.35$ m, in which case $h_{backfill} \geq 0.8$ m is required. Similarly, for $S = 0.45$ m, the backfill thickness must be at least 0.5 m. The improvement of the ampacity performance when $h_{backfill}$ decreases is done by the increase of w_c and the extra concrete material used when w_c increases. In other words, when the volume of the backfill decreases, the volume of the concrete material increases, and in this way, the required current is achieved. To decide which option is the best, a techno-economic analysis must be done. This same analysis can be done for the cable with an aluminum conductor.

B. Induced voltage on cable sheath results

Considering a nominal current of 900 A, the cables capable of carrying this current, according to Fig. 4, include all copper-conductor cables for every spacing value S. Only those with a cross-section greater than or equal to 1600 mm^2 for aluminum-conductor cables meet the requirement for all S values. Additionally, when S = 450 mm, the aluminum-conductor cable with a 1400 mm^2 cross-section satisfies the current required. Therefore, these cable configurations are considered for further analysis in this subsection.

The induced voltages on the cable sheath due to inductive coupling, for the cables positioned at the extreme of the duct bank, are shown in Fig. 7, considering both copper and aluminum-conductor cables under different values of S. The edge cables are analyzed because, in a flat configuration, they are the ones that exhibit the highest induced voltages [1].

Larger cross-sections reduce the induced voltage on the cable, whereas increasing S leads to higher induced voltages; this latter behavior has also been previously reported in the literature [5]. Lower induced voltages enable longer minor section lengths when applying the CB technique.

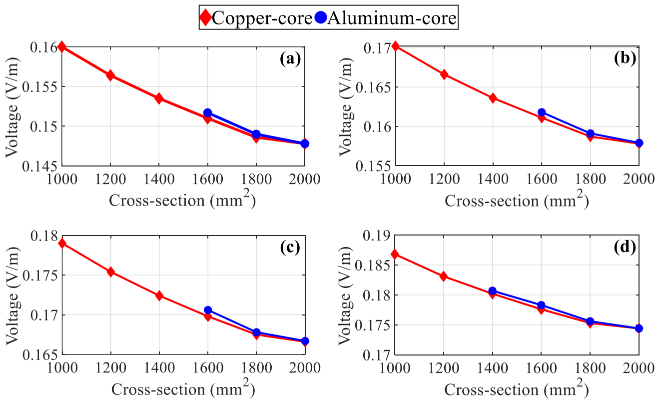

Fig. 7. Induced voltage on cable sheath varying S for I = 900 A. (a) 300 mm, (b) 350 mm, (c) 400 mm, and (d) 450 mm.

Consequently, smaller values of S combined with larger cable cross-sections exhibit the most favorable scenario for achieving longer minor section lengths. However, a larger cable cross-section also entails higher costs. When comparing copper- and aluminum-conductor cables, the difference in induced voltage for the same cross-section is relatively small, with aluminum-conductor cables exhibiting slightly higher values.

In these conditions, the smallest copper-conductor cable that satisfies the ampacity requirement has a 1000 mm^2 cross-section, while for aluminum-conductor cables, the minimum viable option is 1600 mm^2. The aluminum option makes it possible to reach slightly longer minor sections. For instance, with a 100 V limit, the copper-conductor cable allows up to 625 m, whereas the aluminum-conductor cable extends this to 659 m.

V. Conclusions

This paper has comprehensively analyzed how the surrounding media influences the ampacity and the induced voltages on the cable sheath. The study focused on a 220 kV single-circuit underground transmission line arranged in a flat duct-bank configuration, where the ducts are embedded in concrete and a controlled backfill layer is applied above the duct bank to enhance the thermal performance. Different cable cross-sections with copper and aluminum conductors were evaluated, along with variations in cable spacing, natural ground thermal resistivity, and the depth of the backfill layer.

The results demonstrate that, on average, copper-conductor cables provide approximately 185 A higher ampacity than aluminum-conductor cables. This implies that a copper-conductor cable with a smaller cross-section can achieve equivalent thermal performance to an aluminum-conductor cable with a significantly larger cross-section. For instance, in the case study considered, a 1000 mm^2 copper-conductor cable and a 1600 mm^2 aluminum-conductor cable can transport 900 A without exceeding the thermal limit. However, this thermal advantage exhibited by the copper-conductor cables comes at the expense of higher induced sheath voltages and, probably, higher costs for the project. This trade-off must be carefully considered in practical design and operation.

Therefore, in practical design, the choice between copper and aluminum conductors should not rely solely on thermal performance but should integrate a techno-economic assessment that accounts for construction costs, expected loading conditions, induced voltage management, and long-term operational reliability.

References

[1] J. E. G. Asorza, R. A. d. Araujo, J. S. L. Colqui, and J. P. Filho, "Techno-economic analysis of single-circuit underground transmission line duct banks," in *2024 IEEE URUCON*, 2024, pp. 1–5.

[2] IEC 60287-1-1, "Electric cables - calculation of the current rating - part 1-1: Current rating equations (100 % load factor) and calculation of losses - general," Standard, 2023.

[3] Cigre Working Group B1.56, "Power cable rating examples for calculation tool verification," CIGRE, Technical Brochure 880, 2022.

[4] F. de Leon and G. J. Anders, "Effects of backfilling on cable ampacity analyzed with the finite element method," *IEEE Trans. Power Del.*, vol. 23, no. 2, pp. 537–543, 2008.

[5] J. E. G. Asorza, J. S. Leon Colqui, S. Kurokawa, and J. P. Filho, "Analysis of increased induced voltages on the sheath of double-circuit underground transmission lines guaranteeing ampacity," *Energies*, vol. 17, no. 7, 2024.

[6] J. E. G. Asorza, J. S. L. Colqui, R. A. de Araujo, J. P. Filho, and S. Kurokawa, "Impact of underground obstructions in double-circuit underground power lines: Ampacity and induced effect," *IEEE Trans. Indus. Appl.*, pp. 1–12, 2025.

[7] "CYMCAP version 8.1 for Windows, CYME Int. T&D, Dec. 2017 St. Bruno, QC, Canada," https://www.cyme.com/, 2017, Accessed: 2023-03-17.

[8] ELEK Software, "ELEK Cable High Voltage – Electrical Cable Calculation Software."

[9] COMSOL AB, "Comsol multiphysics® v. 6.1," https://www.comsol.com, 2022, stockholm, Sweden.

[10] T. A. Papadopoulos, A. I. Chrysochos, and M. Fotos, "Comparison of power cables current rating calculation methods," in *2023 58th International Universities Power Engineering Conference (UPEC)*, 2023, pp. 1–6.

[11] S. Dubitsky, G. Greshnyakov, and N. Korovkin, "Comparison of finite element analysis to IEC-60287 for predicting underground cable ampacity," in *2016 IEEE International Energy Conference (ENERGYCON)*, 2016, pp. 1–6.

[12] T. A. Papadopoulos, A. I. Chrysochos, C. F. Lazos, I. F. Gonos, K. Pavlou, and G. Georgallis, "Modelling aspects of sheath bonding in medium- voltage cable systems: Operational condition," in *55th International Universities Power Engineering Conference (UPEC)*, 2020, pp. 1–6.

[13] IEEE Std 575, "IEEE Guide for Bonding Shields and Sheaths of Single-Conductor Power Cables Rated 5 kV through 500 kV," pp. 1–83, 2014.

[14] CIGRE WG B1.18, "Special bonding of high voltage power cables," 2005, Technical Brochure 283.

[15] J. E. Guevara, J. S. L. Colqui, and J. P. Filho, "Generalized model for calculating induced voltage on the sheath in steady-state for single-circuit underground transmission lines," in *2024 IEEE Power & Energy Society General Meeting (PESGM)*, 2024, pp. 1–5.

[16] U. S. Gudmundsdottir, "Modelling of long high voltage ac cables in the transmission system," 2010.

[17] P. Ocłoń, P. Cisek, M. Pilarczyk, and D. Taler, "Numerical simulation of heat dissipation processes in underground power cable system situated in thermal backfill and buried in a multilayered soil," *Energy Conversion and Management*, vol. 95, pp. 352–370, 2015.

[18] IEC 60502-1, "Power cables with extruded insulation and their accessories for rated voltages from 1 kV (Um = 1,2 kV) up to 30 kV (Um = 36 kV) - Part 1: Cables for rated voltages of 1 kV (Um = 1,2 kV) and 3 kV (Um = 3,6 kV)," Standard, 2021.

[19] P. Ocłoń, "The effect of soil thermal conductivity and cable ampacity on the thermal performance and material costs of underground transmission line," *Energy*, vol. 231, p. 120803, 2021.

[20] J. E. G. Asorza, J. S. Colqui, F. F. da Silva, and J. P. Filho, "Earth continuity conductor location in single-circuit underground transmission line using the generalized model," *Electr. Power Syst. Res.*, vol. 235, p. 110879, 2024.

[21] M. I. S. L. Simoes, "Contributions to Modeling and Simulation of HVAC Cables Using Field Test Results," PhD Thesis, École Polytechnique de Montréal, Montréal, Canada, 2016.

[22] TF Kable, *High and Extra High Voltage Cables*, TF Kable, n.d., product catalogue.

979-8-3315-8138-1